Staircase model of GaSb(001) (1×3) and $c(2\times6)$ phases

O. Romanyuk,* V. M. Kaganer, R. Shayduk, B. P. Tinkham, and W. Braun
Paul-Drude-Institut für Festkörperelektronik, Hausvogteiplatz 5-7, D-10117 Berlin, Germany
(Received 25 March 2008; revised manuscript received 19 May 2008; published 27 June 2008)

We show that the (1×3) and $c(2\times6)$ diffraction patterns of the reconstructed GaSb(001) surface are the result of characteristic disorder in the positions of the (4×3) reconstructed surface unit cells. The reconstructed cells form uniform rows in the $4\times$ direction with the rows shifted with respect to each other. Random shifts of the rows result in the (1×3) diffraction pattern. If only shifts by $\pm1/4$ between the unit-cell rows are allowed, we obtain the $c(2\times6)$ pattern. Our results agree with the electron counting rule, previous scanning tunneling microscopy studies, and our own reflection high-energy electron-diffraction observations.

DOI: 10.1103/PhysRevB.77.235322 PACS number(s): 68.47.Fg, 68.35.B−, 61.05.jh

The termination of a semiconductor bulk crystal at its surface results in dangling bonds. The surface reconstructs to minimize the number of these dangling bonds and hence the surface energy. A fundamental understanding of the surface reconstructions is therefore necessary to develop smooth, abrupt interfaces for III/V semiconductor devices, since surface reconstructions may lead to anisotropic growth morphologies, causing roughness at a heterointerface, or may produce nonstoichiometric interfaces that are not compositionally abrupt (see e.g., Ref. 1 and references therein).

GaSb is a technologically important direct band gap semiconductor used for photonic applications in the long wavelength range. It is closely lattice-matched to InAs and AlSb, allowing the growth of band gap engineered device heterostructures.[2,3] GaSb features a sequence of surface reconstructions that is different from the other III–V zinc blende structure semiconductors. Several surface reconstructions of GaSb(001) have not been determined until now.

The known diffraction patterns of GaSb(001) are as follows, in the sequence of decreasing temperature. The (1×3) diffraction pattern is observed at typical device growth conditions.[4] This pattern shows clear and intense $3\times$ reflections along the [110] azimuth. At lower temperatures, the (1×3) pattern changes to $c(2\times6)$. The transition is gradual, a mixture of (1×3) and $c(2\times6)$ diffraction patterns is frequently observed.[5,6] Further cooling gives rise to a $5\times$ periodicity in the diffraction pattern along the [110] direction. The Sb-rich $5\times$ phases are believed to be metallic and (1×5), $c(2\times10)$, and (2×10) models are discussed.[7]

In this work, we focus on analyzing the (1×3) and $c(2\times6)$ patterns. We show that the (1×3) and $c(2\times6)$ diffraction patterns are compatible with the (4×3) unit cell. They arise due to different types of one-dimensional disorder between unit cell rows. To verify our model, we prepare both GaSb(001)$-(1\times3)$ and $c(2\times6)$ structures by molecular beam epitaxy (MBE) and determine their in-plane diffraction patterns by reflection high-energy electron diffraction (RHEED) azimuthal scans.

Figure 1 shows azimuthal reflection high-energy electron-diffraction (RHEED) scans of these two surface symmetries. Such a top view of the reciprocal lattice is produced by acquiring the diffracted intensity along a line parallel to the shadow edge in RHEED while azimuthally rotating the sample. The intensity map is then obtained by plotting this linear intensity in the plane parallel to the surface according to its azimuthal recording angle.[8,9] The GaSb(001) (1×3) and $c(2\times6)$ phases were prepared by MBE. Typical ultrahigh vacuum (UHV) conditions were used. The chamber pressure was around 10^{-9} mbar during the measurements. We used unintentionally doped p-type GaSb(001) $\pm0.02°$ wafers. After oxide desorption under a constant Sb flux, the Ga cell was opened to grow a buffer layer with a constant III/V flux ratio of approximately 1:3. The growth rate was determined from RHEED growth oscillations to 1 nm/min. The substrate temperature was kept constant at 526 ± 5 °C and 467 ± 5 °C for the (1×3) and $c(2\times6)$ phases, respectively. RHEED patterns were acquired during azimuthal scans with constant rotation speed and fixed incidence angle of the electron beam. The primary beam energy was 20 keV. The images were generated and acquired using a commercial RHEED data acquisition and processing software.[10] The results are shown in Fig. 1. Figure 1(a) shows the (1×3) phase and Fig. 1(b) the $c(2\times6)$ phase. The (1×1) unit cell is marked by a dashed square. The additional rows of centered spots along the horizontal direction half way between the bright $3\times$ rows are clearly visible in Fig. 1(b).

The structure model of the (1×3) reconstruction,[11] proposed on the basis of photoemission and scanning tunneling microscopy (STM) measurements, consists of Sb dimer rows along $[\bar{1}10]$ separated by a row of Ga. In STM, partial disorder and zigzag features of the dimer rows are observed. A structure model with a $c(2\times6)$ unit cell,[12] based on RHEED

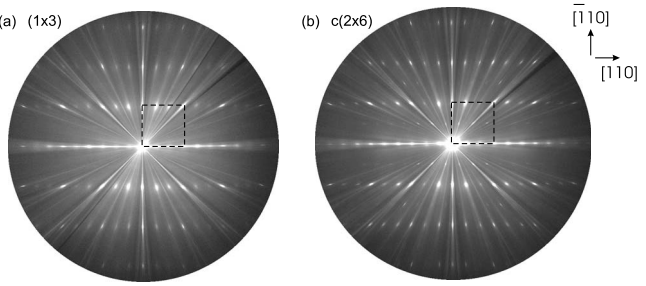

FIG. 1. Azimuthal RHEED scans of a GaSb(001) surface with (a) (1×3) and (b) $c(2\times6)$ symmetry. The Sb flux corresponds to a stoichiometric growth rate of 3 nm/min. Substrate temperature in (a) 526 ± 5 °C and in (b) 467 ± 5 °C.

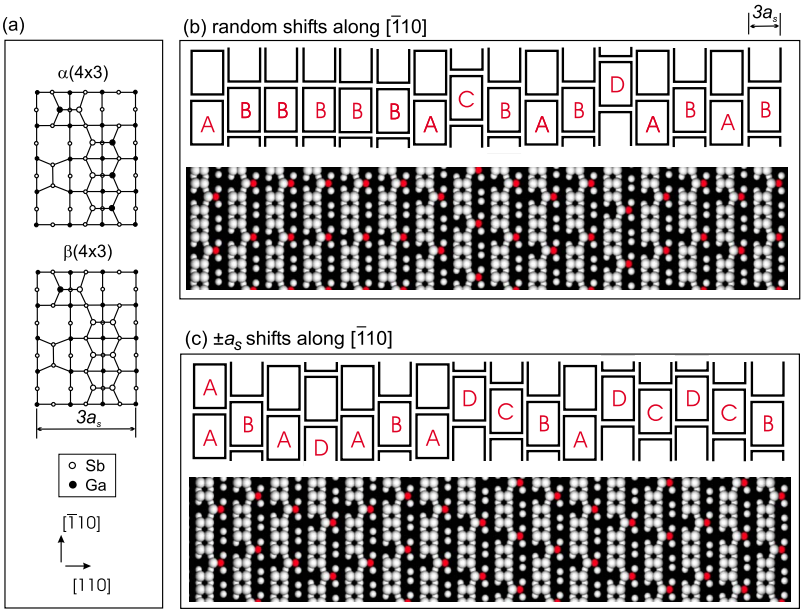

FIG. 2. (Color online) (a) Structure models of the GaSb(001) α and $\beta(4\times3)$ reconstruction. (b),(c) Schematic views of shifted unit cell arrangements with (b) random up and down unit cell shifts and (c) with up and down shifts strictly by one quarter of the reconstructed cell. Only the top 2 ML of GaSb are shown in (b),(c). The bright and dark (red online) spheres are Sb and Ga atoms, respectively. The structure motifs were taken from the arrangements that were used in the structure factor calculations.

and photoemission studies, terminates the surface by an Sb dimer row, similar to the (1×3) model, but without a row of Ga. The $c(2\times6)$ periodicity is created by Sb dimers in the second layer. These two models do not obey the electron counting rule.[13] This rule allows the identification of probable structure models by simply counting the electrons within a surface unit cell. It determines the surface to be semiconducting and charge neutral by counting the number of III–III, V–V bonds and the number of dangling bonds of group III and group V elements. Both above mentioned models could not be confirmed by density functional theory (DFT) calculations.[14] We are not aware of any other structure models based on a (1×3) or $c(2\times6)$ unit cell. The reconstructions of AlSb(001) and GaSb(001) are very similar. Both materials have similar lattice constants (0.7% difference) and produce the same (1×3) and $c(2\times6)$ diffraction patterns, which exist in similar temperature ranges.[15] STM studies[16,17] find a (4×3) unit cell for both the GaSb(001) and AlSb(001) reconstructions. Two phases can be distinguished, α and β. Subsequent DFT calculations[14] indicate that the (4×3) unit cell has the lowest surface formation energy for both the AlSb(001) and GaSb(001) reconstructions. The most likely structures of the GaSb(001)$-(4\times3)$ unit cells are shown in Fig. 2(a). The α phase involves four Ga-Sb dimers on top of an Sb layer. The β phase is more Sb-rich and has three Sb-Sb dimers and one Sb-Ga dimer on top of the Sb layer. Both structures satisfy the electron counting rule and have smaller surface formation energies than both the (1×3) and $c(2\times6)$ models. However, despite the microscopic observation and theoretical stability of the (4×3) surface reconstructions, a GaSb(001)$-(4\times3)$ diffraction pattern is not observed in the diffraction experiments (Fig. 1).

A (4×3) surface unit cell spans $4\times3=12$ elementary surface cells. An elementary cell of the truncated bulk zinc blende crystal is defined by the square with the sides along the bulk $[110]$ and $[\bar{1}10]$ directions and an edge length of $a_s=a_b/\sqrt{2}$, where a_b is the bulk lattice constant. The (4×3) cell can therefore be placed on the bulk crystal underneath in 12 nonequivalent positions. This produces 12 translational domains and the corresponding antiphase boundaries between the domains. The STM images of GaSb(001) and AlSb(001)[16–18] show that the unit cells form rows, i.e., there are very few phase boundaries along the $\times3$ direction. On the other hand, the rows shift rather freely with respect to each other in the $4\times$ direction, implying that the corresponding domain boundary energy is small.

Figures 2(b) and 2(c) sketch possible arrangements of the rows by introducing different types of disorder in the relative positions of the rows. Let A, B, C, D be four possible positions of the surface unit cell obtained through an integer number of shifts in the $4\times$ direction by 1/4 of the surface unit cell spacing (or equivalently, by one unit cell of the unreconstructed surface). Figure 2(b) illustrates the case of random shifts: The neighbor of an A row is, with equal probability, an A, B, C, or D row. Figure 2(c) presents another type of disorder, which involves only relative shifts between rows by 1/4 of the surface unit cell. In this case, the neighbors of a row A are either B or D, the neighbors of B are A or C, and so on. Our aim now is to show that each type of disorder gives rise to either the (1×3) or the $c(2\times6)$ diffraction pattern, respectively.

In the calculation of the diffraction patterns, we restrict ourselves to the kinematical approximation. It is well known that the kinematical approximation is generally not sufficient to simulate RHEED intensities since dynamical (multiple scattering) effects are strong in the diffraction of high-energy electrons.[19] However, we are interested in the superlattice reflections of the reconstructed unit cell that originate from very few atomic layers at the surface and are therefore less prone to dynamical effects. Besides that, our primary interest is the symmetry of the diffraction pattern, rather than the precise calculation of the intensities.

An ideal periodic repetition of the reconstructed unit cells gives rise to a two-dimensional crystal with a scattering amplitude[20]

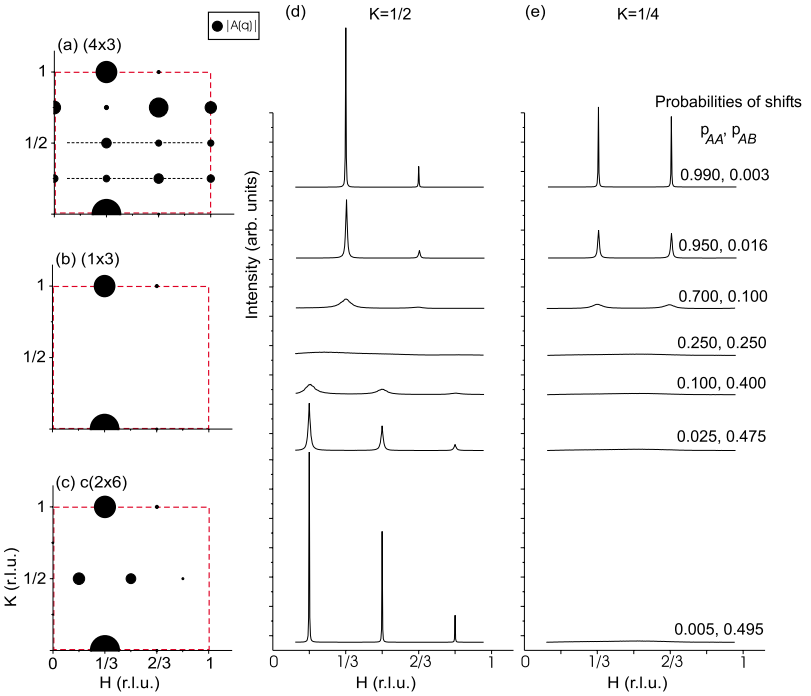

FIG. 3. (Color online) Kinematically calculated GaSb(001) $\beta(4\times3)$ in-plane structure factors for various surface reconstructions. (a) Ideal periodic repetition of the reconstructed unit cell, $p_{AA}=1$, and (b),(c) two types of disorder corresponding to Figs. 2(b) and 2(c) with $p_{AA}=p_{AB}=0.25$ and $p_{AB}=p_{AD}=0.5$, respectively. The areas of the circles are proportional to the intensities of the corresponding reflections. Integer order (bulk) reflections are not shown because of their high intensities. The (1×1) unit cell is marked by the dashed square. Intensity profiles along the lines (d) $K=1/2$ and (e) $K=1/4$, calculated with different probabilities of shifts, p_{AA}, p_{AB}.

$$A(\mathbf{q}) = \sum_{n_1,n_2} F(\mathbf{q})\exp[i\mathbf{q}\cdot(n_1\mathbf{a}_1 + n_2\mathbf{a}_2)], \quad (1)$$

where the sum is performed over the two-dimensional Bravais lattice and $F(\mathbf{q})$ is the scattering amplitude of the single unit cell,

$$F(\mathbf{q}) = \sum_l f_l \exp[i\mathbf{q}\cdot\mathbf{r}_l]. \quad (2)$$

Here, f_l are the atomic scattering factors of the atoms l, $\mathbf{r}_l$ are the positions of atoms within the reconstructed unit cell, $\mathbf{a}_1=(3a_s,0)$ and $\mathbf{a}_2=(0,4a_s)$ are the lattice vectors of the (4×3) cell, and n_1, n_2 are integers. The sum (1) gives rise to the Bragg peaks at the wave vectors $\mathbf{q}=2\pi(m_1/a_1,m_2/a_2)$, where m_1, m_2 are integers. Expressed in units of the surface lattice parameter a_s, the wave vectors are $\mathbf{q}=2\pi(m_1/3a_s,m_2/4a_s)$.

The first type of disorder, shown in Fig. 2(b), is a random shift of each row of (4×3) cells in the $4\times$ direction by multiples of the fundamental a_s spacing, i.e, by $\mathbf{t}_n=n\mathbf{a}_2/4$. There are four independent shifts, $n=0,1,2,3$. When calculating $F(\mathbf{q})$ by Eq. (2), the shifts are taken into account by the substitution $\mathbf{r}_l\rightarrow\mathbf{r}_l+\mathbf{t}_n$ and provide additional phase factors $\exp(i\mathbf{q}\cdot\mathbf{t}_n)$. Since all four displacements occur with equal probabilities, the sum (1) is multiplied by the factor

$$\frac{1}{4}(1 + e^{i\mathbf{q}\cdot\mathbf{a}_2/4} + e^{i\mathbf{q}\cdot\mathbf{a}_2/2} + e^{3i\mathbf{q}\cdot\mathbf{a}_2/4}). \quad (3)$$

Substituting $\mathbf{q}$, we can rewrite this factor as

$$\frac{1}{4}(1 + e^{i\pi m_2/2} + e^{i\pi m_2} + e^{3i\pi m_2/2}). \quad (4)$$

It is equal to 1 for $m_2=0,4,8,\ldots$ and 0 for all other integer values m_2 that are not multiples of 4. In terms of the reconstructed unit cell, only integer order reflections survive along the $4\times$ direction. The resulting diffraction pattern has (1×3) symmetry. It is shown in Fig. 3(b).

The second type of disorder, Fig. 2(c), involves relative shifts of the neighboring rows of unit cells by $\pm\mathbf{a}_2/4$. It corresponds to the AB, BC, DC, etc. states. A similar disorder involving random shifts by a quarter of the surface unit cell is known for the GaAs(001)$-(2\times4)$ reconstruction.[21,22] Let us assume that the first row is in position A. Then, the position of the next row is, with equal probability, either B or D, i.e., it is shifted with respect to the first row by $\pm\mathbf{a}_2/4$. The next row is either A or C, and is shifted with respect to the first row by either 0 or $\mathbf{a}_2/2$. Continuing further, one finds that all odd rods are shifted with respect to the first rod by $\pm\mathbf{a}_2/4$ and all even rods by either 0 or $\mathbf{a}_2/2$, with equal probabilities. It is therefore advantageous to count unit cell rows by pairs and perform the summation using $2\mathbf{a}_1$ instead of $\mathbf{a}_1$ in Eq. (1). A pair of rows with the first row in position A and the second in B or D give rise, on average, to an additional factor in the sum (1),

$$1 + \frac{1}{2}e^{i\mathbf{q}\cdot\mathbf{a}_1}(e^{i\mathbf{q}\cdot\mathbf{a}_2/4} + e^{-i\mathbf{q}\cdot\mathbf{a}_2/4}). \quad (5)$$

If the reference row is in position C rather than A, an additional phase factor $\exp(i\mathbf{q}\cdot\mathbf{a}_2/2)$ arises. When A and C positions are equally probable, Eq. (5) is multiplied by an additional factor,

$$\frac{1}{2}(1 + e^{i\mathbf{q}\cdot\mathbf{a}_2/2}). \quad (6)$$

Now we take into account that we have doubled the period along $\mathbf{a}_1$ and collect the factors (5) and (6) for the wave vectors $\mathbf{q}=2\pi(m_1/2a_1,m_2/a_2)$ to obtain

$$\frac{1}{2}(1+e^{i\pi m_2})\left[1+\frac{1}{2}e^{i\pi m_1}(e^{i\pi m_2/2}+e^{-i\pi m_2/2})\right]. \quad (7)$$

The first term allows only reflections with even m_2. The second term is nonzero only if $m_1=0,2,4,\ldots$ for $m_2=0,4,8,\ldots$ and $m_1=1,3,5,\ldots$ for $m_2=2,6,10,\ldots$. The resulting diffraction pattern has the $c(2\times6)$ symmetry and is shown in Fig. 3(c).

We verify the analytical results by a direct numerical calculation of the scattering from a large ensemble of surface unit cells with different types of disorder. In doing so, we can follow the continuous transformation from one type of disorder to the other by varying the probabilities of the shifts. Figures 2(b) and 2(c) show typical arrangements of the unit cells. We obtain the atomic coordinates in the $\beta(4\times3)$ cell from first principles using density functional theory.[23,24] The thickness of the cell is five monolayers of GaSb, which is approximately the penetration depth of RHEED electrons. The atomic scattering amplitudes, $f_l(\mathbf{q})$, are calculated using the tabulated Doyle-Turner scattering factors.[19] The size of the simulated domain is 120 surface unit cells, which approximately corresponds to the coherence length of RHEED. The intensities calculated for such a domain are averaged over 10^3 repetitions generated at random with the same probabilities.

The probabilities p_{AA} to have adjacent rows without a shift, p_{AB} and p_{AD} to have a shift by 1/4 of the surface unit cell either up or down, and p_{AC} to have a shift by 1/2 of the surface unit cell are related by $p_{AA}+p_{AB}+p_{AC}+p_{AD}=1$. We consider only equal probabilities of up and down shifts, $p_{AB}=p_{AD}$. In case they were unequal, the diffraction peaks would deviate from their symmetric positions,[22] a phenomenon which is outside the scope of the present paper. Hence, there are only two independent probabilities, which we denote as p_{AA} and p_{AB}.

Figures 3(d) and 3(e) show the diffracted intensities along the lines $K=1/2$ and $K=1/4$ in reciprocal space (HK are continuous Miller indices). The top curves correspond to almost perfect (4×3) order: The probability $p_{AA}=0.99$ produces a mean size of AAAA… domains equal to $1/(1-p_{AA})=100$, while the probabilities of the AB, AC, and AD shifts are equal. Figure 3(a) shows the (4×3) diffraction pattern obtained from such a configuration. The radii of the dots in Figs. 3(a)–3(c) are proportional to the scattering amplitudes $|A(\mathbf{q})|$ so that the areas of the dots represent intensities $|A(\mathbf{q})|^2$. As the probability p_{AA} decreases, the diffraction peaks broaden and become less intense. For a probability $p_{AA}=0.95$ (a mean domain size of 20 unit cells), the peaks are still intense and sharp. Only when the probability decreases to 0.7 (mean domain size 3.33 unit cells), the diffraction peaks have low intensity and become difficult to detect experimentally. In the kinematical calculations, the integrated intensity of the peaks is constant (proportional to the number of scatterers), so that, as the disorder is increased, the intensity redistributes from the narrow and intense peaks into wide ones with low intensity. Such peaks are hard to distinguish from a diffuse background in the experiment. Finally, in the case of a complete disorder of (4×3) unit cells, $p_{AA}=0.25$, the $K=1/2$ and $K=1/4$ diffraction peaks are too broad to be distinguished from the background. The diffraction pattern is (1×3) [Fig. 3(b)], in agreement with the analytical calculations above.

As the probability p_{AB} increases further, the $\pm1/4$ shifts begin to dominate. Such a kind of order gives rise to sharp $(n/6,1/2)$ peaks as seen in the bottom curves in Fig. 3(d). On the other hand, the reflections along $K=1/4$ remain very weak and broad and cannot be distinguished from the background [Fig. 3(e)]. This arrangement produces the $c(2\times6)$ symmetry as shown in Fig. 3(c).

Thus, we have demonstrated that the (1×3) and $c(2\times6)$ diffraction patterns are due to different types of disorder of the (4×3) surface reconstructed unit cell rows and not due to a change in symmetry of the basic surface unit cell. Random shifts of the rows by $\pm1/4$ with respect to the adjacent rows along the $4\times$ direction give rise to the centered $c(2\times6)$ diffraction pattern. This is the low-temperature phase observed by RHEED [Fig. 1(b)]. Higher substrate temperatures result in an increased disorder, where all rows are randomly shifted along the $4\times$ direction with respect to each other. This high-temperature configuration produces the (1×3) diffraction pattern [Fig. 1(a)]. Our model agrees with the published STM measurements, where partial disorder was observed.[1,16,18] It explains the experimentally observed RHEED patterns using the energetically favorable surface unit cell, and agrees with the electron counting rule.

The authors would like to thank Steffen Behnke for technical assistance and Dillip Kumar Satapathy for help with the RHEED measurements.

*On leave from Institute of Physics of the ASCR, v. v. i.; romanyuk@fzu.cz

[1] P. M. Thibado, B. R. Bennett, B. V. Shanabrook, and L. J. Whitman, J. Cryst. Growth **175-176**, 317 (1997).
[2] R. J. Malik, J. P. van der Ziel, B. F. Levine, C. G. Bethea, and J. Walker, J. Appl. Phys. **59**, 3909 (1986).
[3] A. G. Milnes and A. Y. Polyakov, Solid-State Electron. **36**, 803 (1993).
[4] A. S. Bracker, M. J. Yang, B. R. Bennett, J. C. Culbertson, and W. J. Moore, J. Cryst. Growth **220**, 384 (2000).
[5] M. T. Sieger, T. Miller, and T.-C. Chiang, Phys. Rev. B **52**, 8256 (1995).
[6] Q.-K. Xue, T. Hashizume, and T. Sakurai, Prog. Surf. Sci. **56**, 1 (1997).
[7] L. J. Whitman, P. M. Thibado, S. C. Erwin, B. R. Bennett, and B. V. Shanabrook, Phys. Rev. Lett. **79**, 693 (1997).
[8] W. Braun, H. Möller, and Y. H. Zhang, J. Vac. Sci. Technol. B **16**, 1507 (1998).
[9] O. Romanyuk, K. Kataoka, F. Matsui, K. Hattori, and H. Daimon, Czech. J. Phys. **56**, 267 (2006).

[10] SAFIRE RHEED measurement and analysis software by Createc GmbH Fischer & Co. GmbH (www.createc.de).
[11] G. E. Franklin, D. H. Rich, A. Samsavar, E. S. Hirschorn, F. M. Leibsle, T. Miller, and T.-C. Chiang, Phys. Rev. B **41**, 12619 (1990).
[12] F. Maeda, Y. Watanabe, and M. Oshima, J. Electron Spectrosc. Relat. Phenom. **80**, 225 (1996).
[13] M. D. Pashley, Phys. Rev. B **40**, 10481 (1989).
[14] M. C. Righi, R. Magri, and C. M. Bertoni, Phys. Rev. B **71**, 075323 (2005).
[15] M. Yano, H. Yokose, Y. Iwai, and M. Inoue, J. Cryst. Growth **111**, 609 (1991).
[16] W. Barvosa-Carter, A. S. Bracker, J. C. Culbertson, B. Z. Nosho, B. V. Shanabrook, L. J. Whitman, H. Kim, N. A. Modine, and E. Kaxiras, Phys. Rev. Lett. **84**, 4649 (2000).
[17] A. S. Bracker, B. Z. Nosho, W. Barvosa-Carter, L. J. Whitman, B. R. Bennett, B. V. Shanabrook, and J. C. Culbertson, Appl. Phys. Lett. **78**, 2440 (2001).
[18] U. Resch-Esser, N. Esser, B. Brar, and H. Kroemer, Phys. Rev. B **55**, 15401 (1997).
[19] A. Ichimiya and P. I. Cohen, *Reflection High Energy Electron Diffraction* (Cambridge University Press, Cambridge, 2004).
[20] B. E. Warren, *X-Ray Diffraction* (Dover, New York, 1990).
[21] Y. Garreau, M. Sauvage-Simkin, N. Jedrecy, R. Pinchaux, and M. B. Veron, Phys. Rev. B **54**, 17638 (1996).
[22] M. Takahasi, Y. Yoneda, N. Yamamoto, and J. Mizuki, Phys. Rev. B **68**, 085321 (2003).
[23] The ABINIT code is a common project of the Université Catholique de Louvain, Corning Incorporated, and other contributors (www.abinit.org).
[24] X. Gonze *et al.*, Comput. Mater. Sci. **25**, 478 (2002).